Imaging and Dosimetry Study of Inter-fraction Setup Error in a Murine Xenograft Flank Tumor Radiation Model

Authors: Smith, Emily J., Tryggestad, Erik J., Carlson, Brett L., Walb, Matthew C., and Sarkaria, Jann N.

Source: Radiation Research, 193(2) : 161-170

Published By: Radiation Research Society

URL: https://doi.org/10.1667/RR15526.1

RADIATION RESEARCH **193**, 161–170 (2020)
0033-7587/20 $15.00

DOI: 10.1667/RR15526.1

Imaging and Dosimetry Study of Inter-fraction Setup Error in a Murine Xenograft Flank Tumor Radiation Model

Emily J. Smith,[2,3] Erik J. Tryggestad,[1,2] Brett L. Carlson, Matthew C. Walb[4] and Jann N. Sarkaria

Department of Radiation Oncology, Mayo Clinic Rochester, Rochester, Minnesota 55905

Smith, E. J., Tryggestad, E. J., Carlson, B. L., Walb, M. C. and Sarkaria, J. N. Imaging and Dosimetry Study of Inter-fraction Setup Error in a Murine Xenograft Flank Tumor Radiation Model. *Radiat. Res.* 193, 161–170 (2020).

Modern small animal irradiation platforms provide for accurate delivery of radiation under 3D image guidance. However, leveraging these improvements currently comes at the cost of lower-throughput experimentation. Herein, we characterized setup accuracy and dosimetric robustness for mock/sham irradiation of a murine xenograft flank tumor model using the X-RAD SmART+ with the vendor-supplied Monte Carlo (MC) treatment planning system (SmART ATP). The chosen beam arrangement was parallel-opposing using a 20 mm square collimator, aligned off-axis for ipsilateral lung sparing. Using a cohort of five mice imaged with cone beam computed tomography (CBCT) over five consecutive mock-irradiation fractions, we compared inter-fraction setup variability resulting from a vendor-supplied multi-purpose bed with anesthesia nose cone with a more complicated immobilization solution with an integrated bite block with nose cone and Styrofoam platform. A hypothetical "high-throughput" image-guidance scenario was investigated, wherein the day 1 stage coordinates (resulting from CBCT guidance) were applied on days 2–5. Daily inter-fraction setup errors were evaluated per specimen (days 2–5) using CBCT-derived offsets from day 1 stage coordinates. Using the CBCT images and Monte Carlo dose calculation, 3D dosimetric plan robustness was evaluated for the vendor-supplied immobilization solution, for both the high-throughput guidance scenario as well as for use of daily CBCT-based alignment. Inter-fraction setup offset magnitude was 3.6 (±1.5) mm for the vendor-supplied immobilization compared to 3.3 (±1.8) mm for the more complicated solution. For the vendor-supplied immobilization, we found that daily CBCT was needed to adequately cover the flank tumors dosimetrically, given our chosen treatment approach. © 2020 by Radiation Research Society

INTRODUCTION

Sophisticated preclinical radiation models are becoming more commonplace with the development of ''micro-irradiators''. However, understanding how these systems can be optimally integrated into medium- to high-throughput preclinical animal testing has not been adequately addressed. Previously, at our institution and elsewhere, high-throughput radiation studies were performed using cesium irradiators, which required custom lead blocks for both targeting and collimation. Such a radiation delivery system necessitated relatively large irradiation fields due to relatively crude block placement. Moreover, use of single beam portals resulted in relatively heterogenous dose coverage due to X-ray attenuation with depth. In contrast, more modern stereotactic animal irradiation systems are equipped with on-board 3D imaging for guidance and planning software, allowing for increasingly conformal dose distributions. These systems, therefore, better mimic modern clinical techniques, theoretically improving clinical translation (*1*). However, direct translation of clinical workflows back into the preclinical setting is severely limited by the competing demands of high-throughput preclinical experimentation. Such demands, in practice, preclude the typical clinical patient- or subject-specific workflow involving pre-treatment imaging, treatment planning, multiple- (25–35) fraction delivery and a quality assurance paradigm of monitoring dosimetric plan robustness over the course of treatment. Thus, we find ourselves having better tools for preclinical radiation models, but, in practice, we struggle to apply these tools to the level of their designed potential.

Our group acquired an X-RAD SmART+ image-guided small animal irradiator (Precision X-ray Inc., North Bradford, CT) in 2017. Since that time, efforts have been ongoing to characterize achievable accuracy and radiation dosimetry in the context of more practical, higher-

[1] Address for correspondence: Department of Radiation Oncology, Mayo Clinic, 200 First Street SW, Rochester, MN 550905; email: Tryggestad.Erik@mayo.edu.
[2] These authors contributed equally to this work.
[3] Current affiliation: Carle Illinois College of Medicine, University of Illinois, Champaign, IL 61820.
[4] Current affiliation: Department of Radiation Oncology and Winship Cancer Institute, Emory University, Atlanta, GA 30322.

throughput experimentation. One major focus of our group is that of brain tumor models; thus, the first study performed by our group examined setup reproducibility for irradiation of intracranial tumors (*2*). Here, we reported minimal variation in inter-subject setup position, allowing for the stereotactic coordinates of a single mouse (determined from image-guided target placement of the first mouse subject) to be applied to all the subsequent mice in a cohort for a given fraction. We maintained confidence that we could directly translate this derived geometric uncertainty to dosimetric robustness in the context of the chosen beam collimation; this confidence was derived from the stereotactic approach used for tumor cell transplantation/injection as well as the physical-geometric constraints on tumor growth and shape in the confines of the skull. However, in flank models, tumor growth is less predictable and transplantation is not as easily standardized, both of which result in significant variation in tumor size, shape and location relative to contextual anatomy.

Many radiation oncology preclinical studies utilize xenograft models where the tumor cells are placed subcutaneously into the flank of small rodents. For the current study, we were interested in evaluating achievable targeting and Monte Carlo treatment planning system predicted radiation dosimetry in the context of a practical, higher-throughput, flank tumor irradiation model under development in our laboratory. We sought to describe both setup variability and flank tumor 3D dosimetric plan robustness in the context of this observed setup variation using a generalized fixation system incorporating only a nose cone for anesthesia delivery. Important consideration for this radiation model is normal tissue radiation exposure, as the broader preclinical experimental context is evaluation of chemotherapeutic agents that are potential radiosensitizers. Thus, normal tissue sparing was an important consideration.

MATERIALS AND METHODS

X-RAD SmART+ Irradiation Platform

Aspects of the X-RAD SmART+ irradiation platform used in this study are described elsewhere [e.g., (*1, 3, 4*)]. The system at the Mayo Clinic (Rochester, MN), used in this study, is capable of delivering image-guided radiotherapy (IGRT) using 2D X-ray projection imaging, 3D cone beam CT (CBCT) and 2D optical (bioluminescence) imaging. Therapeutic radiation is delivered with the same X-ray tube as imaging using the maximum available kVp (225) with the larger available focal spot and 0.3 mm of Cu filtration. The system has a high-power generator capable of 20 mA, which delivers >5 Gy/min at an arbitrarily defined calibration depth of 2 cm in water.

Murine Tumor Model

The experiments described herein were performed under a Mayo Clinic Rochester IACUC-approved protocol. Athymic nude mice (N = 5), 7–8 weeks old, were subcutaneously injected with GBM10 cells (approximately 2×10^6 cells per animal, previously incubated in stem cell media) on the right flank overlying the lower, lateral rib cage. Tumors were allowed to grow for 22 days to achieve tumor volumes of greater than 100 mm^3 before the current experiment was started.

Immobilization

Primary: Multiflow bed. Due to convenience and better compatibility with imaging and treatment planning, the interchangeable ''Multiflow'' bed that was purchased as an accessory to the SmART+ system was used as the primary immobilization solution for purposes of 3D dose calculation (see Fig. 1A and B). The Multiflow bed is mainly comprised of a 3D-printed skeleton housing anesthesia and vacuum ports for nose cone delivery and two parallel acrylic plates, with the space between being potentially heated if warm air is supplied on a separate port (not used in the current study). The acrylic plates have combined dose attenuation of 5.6% assuming normal beam incidence (as determined using ion chamber measurements). Each mouse was anesthetized using isoflurane and placed onto the Multiflow bed with the nose positioned in the center of the nose cone and pulled taut from the neck to the tail to straighten the spine as much as possible. The hind legs were then taped down to the stage to minimize subsequent movement.

Secondary: Kopf stereotactic bed. A secondary, investigational immobilization solution was devised for mock flank tumor irradiation based on the Kopf stereotactic bed (model no. 900M; David Kopf Instruments, Tujunga, CA), which we have modified for interchangeability with the PXI robotic stage, as described elsewhere (*2*). The Kopf bed incorporates a bite block into the nose cone used for anesthesia delivery. For this study, the ear pins/bars were not used and were removed; additionally, a Styrofoam block cutout (in the shape of a cross) was included to elevate the body of the mouse and reduce limb interference (see Fig. 1C and D).

CBCT-based Study of Inter-fraction Setup Error

3D target localization. As shown in Fig. 2, a five-day setup and imaging experiment was performed on the X-RAD SmART+ for both the primary and secondary immobilization scenarios. (The same murine subjects were used in both experiments, although the experiments were performed over successive weeks and not conducted simultaneously. Only the primary immobilization solution was considered for CBCT-based dose planning.) On day 1, each of the five mice were localized with fluoroscopic imaging with gantry angles at 0° and 270° to align the flank tumor into the field-of-view for the subsequent CBCT (60 kVp, 0.3 mA, 2.0 mm Al filter, 256 projections and 0.2 mm^3 voxel size). Based on the CBCT, a mock radiation target was set based on surrogate anatomic landmarks independent from the flank tumor, the XYZ stage was shifted, and subsequently the stage positions were recorded and defined as the day 1 coordinates (see Fig. 3). The landmarks used for mock irradiation target localization were the proximal edge of the spinal column (placed at $x = 12.5$ mm), the top layer of the Multiflow bed (placed at $y = -5$ mm) and the center of the visible tumor (placed at $z = 0$ mm). This was repeated on each mouse; hence each mouse was assigned a unique set of day 1 coordinates. On days 2–5, the stage was set to each subject's day 1 coordinates, and a CBCT was taken to capture setup; subsequently, the mock irradiation target was readjusted to the same reference landmarks (as per day 1), and the resultant stage coordinates were recorded (without reimaging). Daily inter-fraction setup error was determined by Cartesian-wise subtraction of final day N (N = 2–5) coordinates from day 1 coordinates. A daily vector offset was derived as $\Delta r = (\Delta x^2 + \Delta y^2 + \Delta z^2)^{1/2}$.

Setup stability: daily transverse angular (or roll) differences. We hypothesized that the secondary immobilization system (defined in Secondary: Kopf stereotactic bed section) might mitigate hind limb interference and reduce the magnitude of daily transverse angle (roll) differences. Roll differences can be appreciated on the top row of Fig. 3 and this is particularly relevant in the context of the mock treatment plan/beam geometry to be described below. To investigate this, images for all five mouse subjects on all five days of mock irradiation, using both immobilization scenarios described in sections ''Primary: Multiflow bed,'' and ''Secondardy:Kopf stereotactic bed'', were

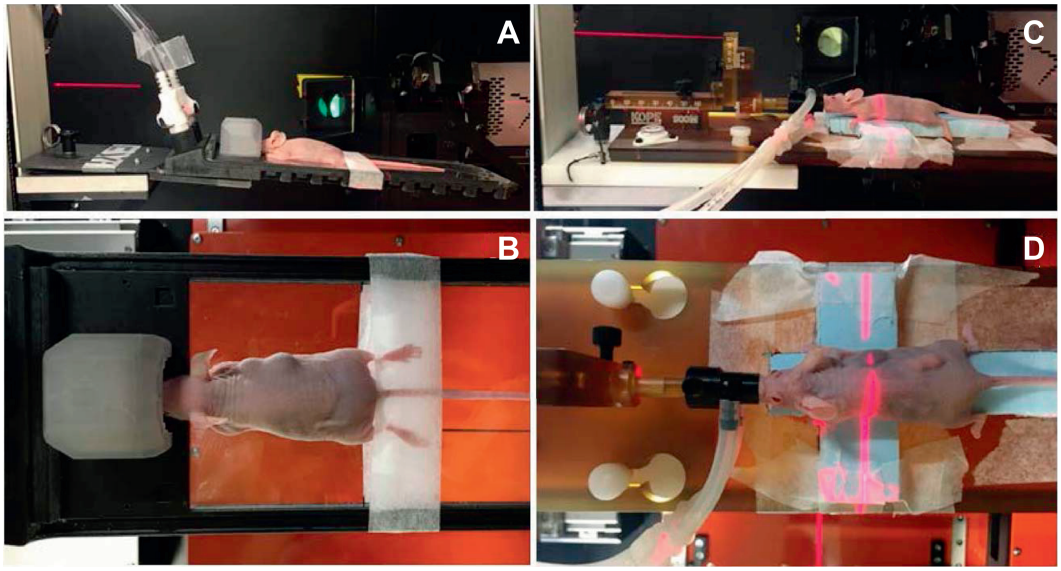

FIG. 1. Immobilization solutions studied here. Side-on (panel A) and top-down (panel B) views of an example subject immobilized using the ''Multiflow'' bed. The same views are shown for the modified Kopf bed immobilization (panels C and D). Isoflurane gas is supplied via the nose cave/cone, as shown.

imported into MIM software, version 6.8.3 (Cleveland, OH). For each immobilization scenario, a rigid, automated ''box-based'' 6D registration was performed between the day 1 and day N image using a manually-positioned 3D region-of-interest over a relevant portion of the spinal column (covering from base of the skull to hind legs). Transverse axis rotations for each immobilization device were recorded and compared on a per-subject and combined basis.

Dose Calculations

1D point dose calculation used for simple radiation prescription. An in-house ''point dose calculator'' (PDC) tool was devised by our medical physics group to enable simple, 1D (single prescription reference point on central beam axis), water-equivalent radiation prescriptions for high-throughput animal experimentation. Implemented as a Microsoft® Excel® macro, the PDC was commissioned using a combination of ion chamber measurements with the reference 4×4 cm^2 collimator and Gafchromic™ EBT3 film (Ashland® Global Holdings Inc., Covington, KY) measurements using stacks of small kV-equivalent solid water (CNMC Company Inc., Nashville, TN) blocks with films located at multiple depths for all available collimator sizes. The stack was exposed at three source-to-surface distances to characterize percentage depth-dose dependency on distance. Film calibration was performed using the reference 4×4 cm^2 collimator at our institution's defined reference calibration depth of 2 cm. This output calibration reference was previously established using an ion chamber following the standardized calibration procedure for 40–300 kVp X-ray beams published by the American Association of Physicists in Medicine (AAPM), Task Group 61 (*5*).

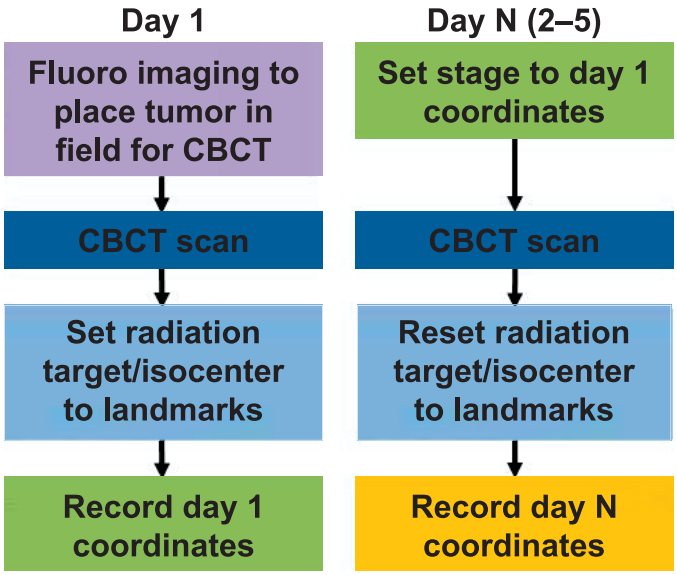

FIG. 2. Workflow for inter-fraction imaging/setup experiments. The differences between day N and day 1 coordinates are indicative of daily 3D setup error.

3D Monte Carlo treatment planning based on CBCT. 3D planning was performed using the ''SmART-ATP'' (Monte Carlo based) treatment planning software version 1.1 (SmART Scientific Solutions B.V., Maastricht, Netherlands) (*6*), which is based on the open-source Monte Carlo dose calculation package EGSnrc/BEAMnrc (*7*). The SmART-ATP system was commissioned independently by the vendor based on their prescribed procedures, also involving combined ion chamber and EBT3 film measurements.

Rather than direct Hounsfield unit (HU) mapping to materials and densities, SmART-ATP employs a HU-thresholding process to define a user-specified set of materials; alternatively, defined materials can be explicitly mapped to contoured structures. Densities are nominally scaled based on a calibrated CBCT HU to density curve, but can also be explicitly overridden to user-specified values per defined material. The material list is preconfigured by the user; numerous standard material/chemical definitions from the ICRU/ICRP are installed with the system by the vendor. For the current study, all CBCT images were segmented into the following vendor-provided standard materials with given CBCT HU limits (in parentheses): air (HU $\leq$ –781), lung (–781 $<$ HU $\leq$ –254), tissue (–254 $<$ HU $\leq$ 501) and bone (HU $>$ 501). The top and bottom (acrylic) plates of the Multiflow bed were contoured and explicitly overridden as polyethylene with nominal density (to approximate acrylic, which was absent from the available materials definition list).

As shown in Fig. 3, the ''off-axis'' isocenter placement for mock irradiation (treatment planning geometry is described below) some-

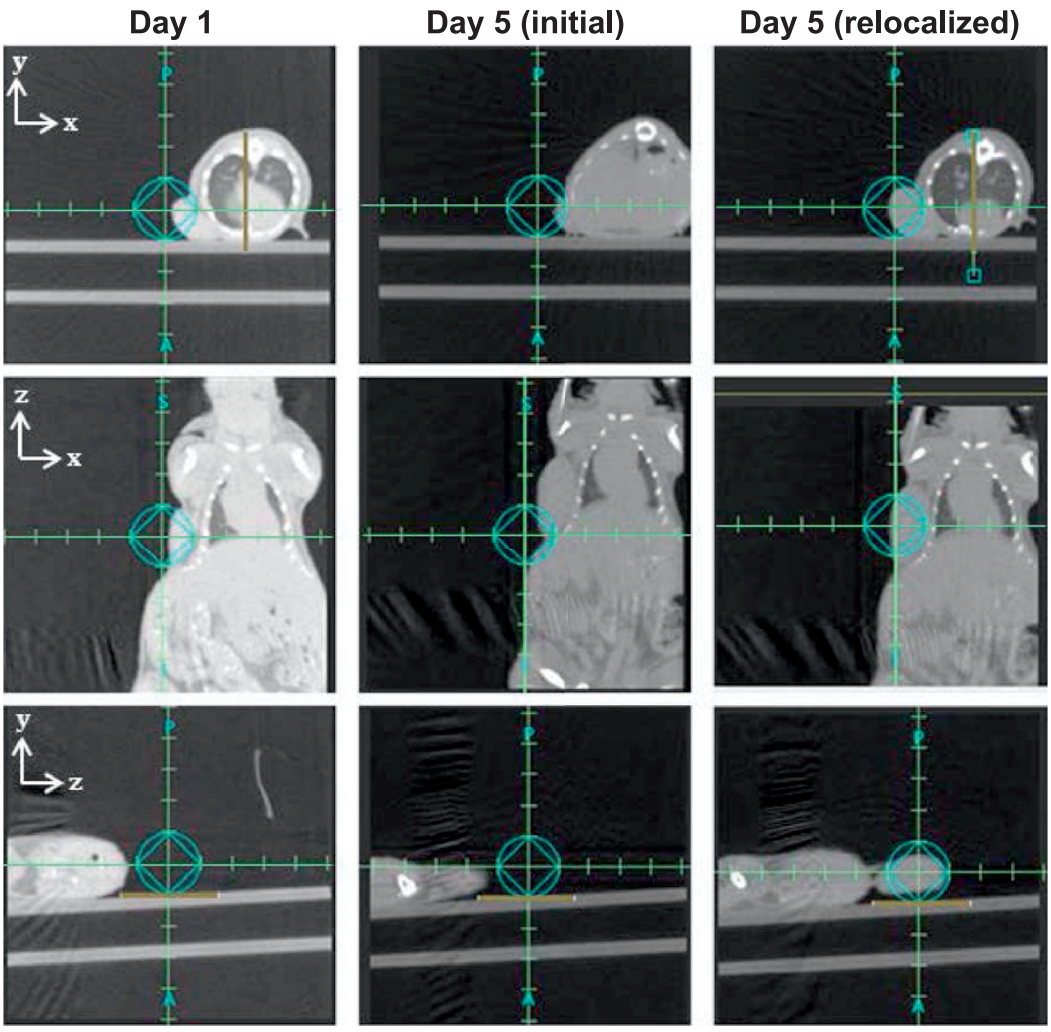

FIG. 3. Example CBCT screen shots (from within the ''Pilot'' control software provided by the vendor) for day 1 vs. day 5 with the Multiflow bed. Left-side column: 3D cut-planes (axial, coronal and sagittal views from top to bottom) showing the target localization (circle with inner diamond) to chosen landmarks on day 1. Middle column: Initial target localization on day 5 scan based on day 1 stage coordinates. Right-side column: Final target location on day 5 based on re-localizing to the given anatomic landmarks. (Cross hair marks are at 5 mm increments; light-brown lines on top and bottom rows reference the surrogate landmarks). Tumor growth has occurred.

times fell outside of the mouse body, in ''air''; due to a limitation in our current version of the SmART-ATP software, dose calculations cannot be produced if the defined isocenter of the CBCT is in ''air.'' When required, a small (and artificial) 3D structure was created around the isocenter location; this structure was overridden as polystyrene with a density override at 0.05 mg/mm^3.

Monte Carlo based treatment plans were calculated with 0.5 mm isotropic dose grid resolution and 3×10^4 phase-space histories/mm^2 per beam, which provided a good tradeoff between speed and accuracy. The choice of the number of phase-space histories was based on an evaluation of convergence of tumor dose-volume histograms (DVHs) (data not shown). In this version of SmART-ATP, dose is prescribed ''automatically'' by specifying a total prescription dose with beam-on times derived based on equal point-dose weighting to isocenter from all fields. Once the dose grids for beams are initially calculated, dose can be re-normalized by entering beam-on times manually, with user input rounded to the nearest second.

Mock treatment beam angle selection. Using a single representative subject's CBCT and Monte Carlo based treatment planning, we evaluated two different contralateral-sparing (or ''off-axis''), parallel-opposing beam arrangements using the 20 mm square collimator. Parallel-opposing beams are useful for high-throughput experimentation because they tend to produce relatively uniform dose distributions along the beam axes (compared to a single field treatment) with a modest efficiency penalty associated with 180° gantry rotation. The first beam arrangement evaluated was anterioposterior-posterioanterior (referred to hereafter as ''AP-PA''), utilizing cardinal gantry angles of 0° and 180°. However, we suspected that an alteration towards an oblique geometry may allow for improved ipsilateral lung sparing. Thus, an ''oblique'' plan employing gantry angles of 340° and 160° was also evaluated.

By convention, beam-on times were specified in the Monte Carlo planning system based on PDC calculations, attempting to achieve a mock irradiation dose of approximately 2.5 Gy per fraction. These ''1D'' PDC calculations necessarily assumed a simplified AP-PA planning geometry, no longer off-axis and based on approximate (assumed water-equivalent) depth-to-isocenter measurements of 5 mm (based on CBCT measurements of tumor midpoint depth in y-direction). Using an exposure setting of 15 s per beam in the PDC

TABLE 1
Inter-fraction (CBCT-derived) Offset Magnitude in mm ± 1 Standard Deviation (Day N–Day 1), where N = 2–5 for Multiflow Bed and Modified Kopf bed with Styrofoam Cutout

	Multiflow bed				Modified Kopf bed (with Styrofoam cutout)			
Mouse ID	|Δx| (mm)	|Δy| (mm)	|Δz| (mm)	Δr (mm)	|Δx| (mm)	|Δy| (mm)	|Δz| (mm)	Δr (mm)
1157	2.7 ± 2.1	0.5 ± 0.2	3.0 ± 0.7	4.3 ± 1.1	1.5 ± 1.5	0.1 ± 0.2	3.9 ± 1.0	4.3 ± 1.5
4883	2.8 ± 1.2	0.2 ± 0.2	1.7 ± 1.3	3.6 ± 0.6	1.1 ± 0.9	0.0 ± 0.0	1.2 ± 1.1	1.7 ± 1.2
6919	1.9 ± 0.7	0.1 ± 0.1	0.8 ± 1.1	2.2 ± 0.9	1.4 ± 1.2	0.0 ± 0.0	0.4 ± 0.5	1.6 ± 1.0
6389	3.0 ± 1.7	0.1 ± 0.1	3.2 ± 2.4	4.5 ± 2.5	3.8 ± 1.2	0.0 ± 0.0	1.5 ± 1.4	4.3 ± 0.9
1784	1.2 ± 1.1	0.1 ± 0.2	2.8 ± 1.9	3.6 ± 0.7	3.8 ± 1.4	0.1 ± 0.1	2.2 ± 1.3	4.5 ± 1.4
Average	2.3 ± 1.5	0.2 ± 0.2	2.3 ± 1.7	3.6 ± 1.5	2.3 ± 1.7	0.0 ± 0.1	1.8 ± 1.6	3.3 ± 1.8
Maximum	4.8	0.6	6.4	7.1	5.6	0.4	5.2	6.3
10th percentile	0.4	0.0	0.0	2.1	0.2	0.0	0.0	0.8
90th percentile	4.1	0.4	3.7	5.3	4.1	0.2	3.5	5.3

Note. Average, maximum, 10th and 90th percentiles are computed with all data points combined (20 samples).

results in a predicted dose of 2.52 Gy (1.3 Gy from the 0° field and 1.22 Gy from the 180° field due to Multiflow bed attenuation). We emphasize that this 15-s beam timer setting was an arbitrary compromise in an attempt to achieve a total experimental prescription dose near 2.5 Gy, in the context of the beam timer rounding issue in the SmART-ATP software.

For both beam arrangements, DICOM CBCT images and Monte Carlo calculated dose were exported to MIM software, where additional contours of the gross tumor volume (GTV) and ipsilateral lung were manually generated. DVHs were comparatively evaluated for GTV coverage and lung sparing.

1D point dose calculator compared with 3D Monte Carlo benchmarking. We designed a benchmarking experiment to elucidate potential inaccuracies in our PDC dose specification, owing to the slightly oblique geometry, and to validate the commissioning process carried out by the vendor for the collimator used in this study (20 mm square). Our PDC necessarily assumes normal beam incidence on water-equivalent (quasi-''infinite'') blocks. As stated in the previous section, for purposes of dose prescription, a representative plan was designed in the PDC using an AP-PA beam arrangement, assuming a 10 mm thick water block (with isocenter placed at the mid-separation depth of 5 mm), allowing that one of the beams first impinged on the Multiflow bed. Similarly, in the 3D Monte Carlo treatment planning system, an analogous (10 mm thick) solid water phantom was created by contouring an appropriate phantom geometry on a blank CBCT scan of the Multiflow bed using a H_2O material override with density override of 1 g/cm^3. The Multiflow bed layers (top and bottom) were contoured and overridden as polyethylene, as described previously. Isocenter was placed in the middle of the phantom, at the mid-separation plane (isocenter depth of 5 mm for both beams). Two treatment plans using a parallel-opposed 20 mm square collimator were generated, namely AP-PA and oblique, both using the same beam-on times specified from the PDC prediction (15 s/beam). For both plans, the number of histories/ mm^2 was increased to 6×10^4, keeping the voxel resolution the same as that used previously (0.5 mm isotropic). Monte Carlo calculated dose at isocenter for both plans was then compared against the PDC ''prescription dose'' of 2.52 Gy.

Planning study of 3D Monte Carlo dosimetric coverage of flank tumors. Focusing on the oblique, off-axis, parallel-opposed beam arrangement described earlier, a treatment plan was calculated for each mouse and each mock treatment fraction, under the two image-guidance scenarios described previously (in the section, CBCT-based Study of Inter-fraction Setup Error), namely, setting up each mouse to day 1 CBCT-derived stage coordinates (no CBCT on days 2–5) compared with acquiring CBCT for every fraction and repositioning the mouse. Calculated dose for each scenario along with CBCT images and the radiotherapy structure set (used to create the described overridden materials) were exported as DICOM to MIM, where the identifiable GTV and the ipsilateral lung were contoured in a consistent fashion on each CBCT. Per-fraction DVHs for these structures for both scenarios were then extracted in tabular format for direct comparison via DVH overlay.

RESULTS

Inter-fraction Setup Reproducibility

3D target localization. Table 1 summarizes our inter-fraction setup reproducibility findings for the mock image-guided irradiation procedure involving use of day 1 stage coordinates, per subject, applied to subsequent days 2–5. The analysis was performed using two immobilization scenarios. For the Multiflow bed, the mean vector offset between the day 1 coordinates and the coordinates for the subsequent days of imaging, combining all subjects' data points, was 3.6 ± 1.5 (±1 SD) mm (N = 20 samples). The more complex immobilization using the modified Kopf platform that incorporates a bite block with a Styrofoam cutout did not significantly improve inter-fraction variation, with a mean vector offset of 3.3 ± 1.8 (±1 SD) mm. The maximum observed daily vector offset was reduced slightly from 7.1 to 6.3 mm with the modified Kopf platform.

Setup stability based on transverse angle (or roll). Figure 4 shows the result for setup stability when looking at transverse angle differences (roll), day N compared with day 1, per subject. On average, no significant or consistent differences were observed. For example, larger rolls were observed in two murine subjects (nos. 6389 and 1784) compared to the other three subjects, likely biasing the average findings.

Dosimetric Findings; Implications of Observed Setup Error

Beam angle selection: AP-PA compared with oblique beam arrangement. Figure 5 shows the mock 3D planning result for an AP-PA beam arrangement compared with a pair of opposing oblique beams. The CBCT imaging data shown was taken from murine subject no. 6389, day 1. The plans were calculated with a 15-s exposure time, per beam (again, the naïve prescription derived via the PDC). As demonstrated by the corresponding DVH analysis, GTV

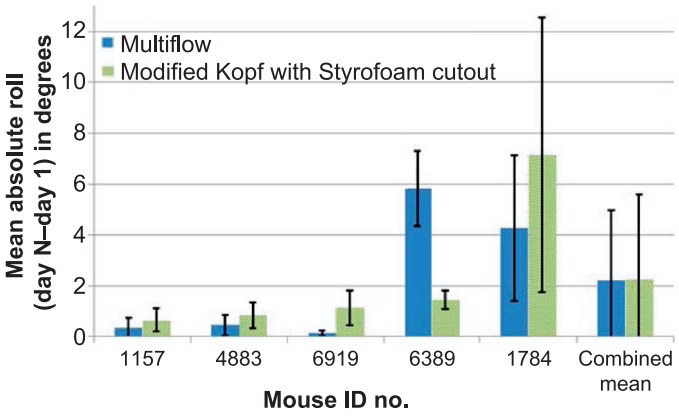

FIG. 4. Mean (±1 SD) absolute transverse angle (roll) differences in degrees, where the day N CBCT was rigidly registered to the day 1 CBCT (N = 2–5), tabulated per subject. The sample size is 20 for the combined data.

dose is similar, whereas more volume of ipsilateral lung is exposed to higher doses with an AP-PA beam arrangement. Renormalization of the AP-PA plan for equivalent target coverage with the oblique scenario would have resulted in a further increase to the ipsilateral lung. Also, note that the field edge is further away from the spinal column in the oblique scenario. Based on these findings, the oblique geometry was preferred for the subsequent Monte Carlo based planning study incorporating daily CBCT imaging for the Multiflow bed (see section below, Flank tumor dose-coverage robustness).

1D point dose calculator compared to 3D Monte Carlo benchmarking. Figure 6A and B shows a transverse cut-plane view through isocenter of the 3D dose distributions resulting from the Monte Carlo treatment plans for the two geometries, namely AP-PA (strictly assumed by the PDC) and oblique. As shown in Fig. 6C, the dose profile, drawn laterally across the high-dose region in the isocentric plane

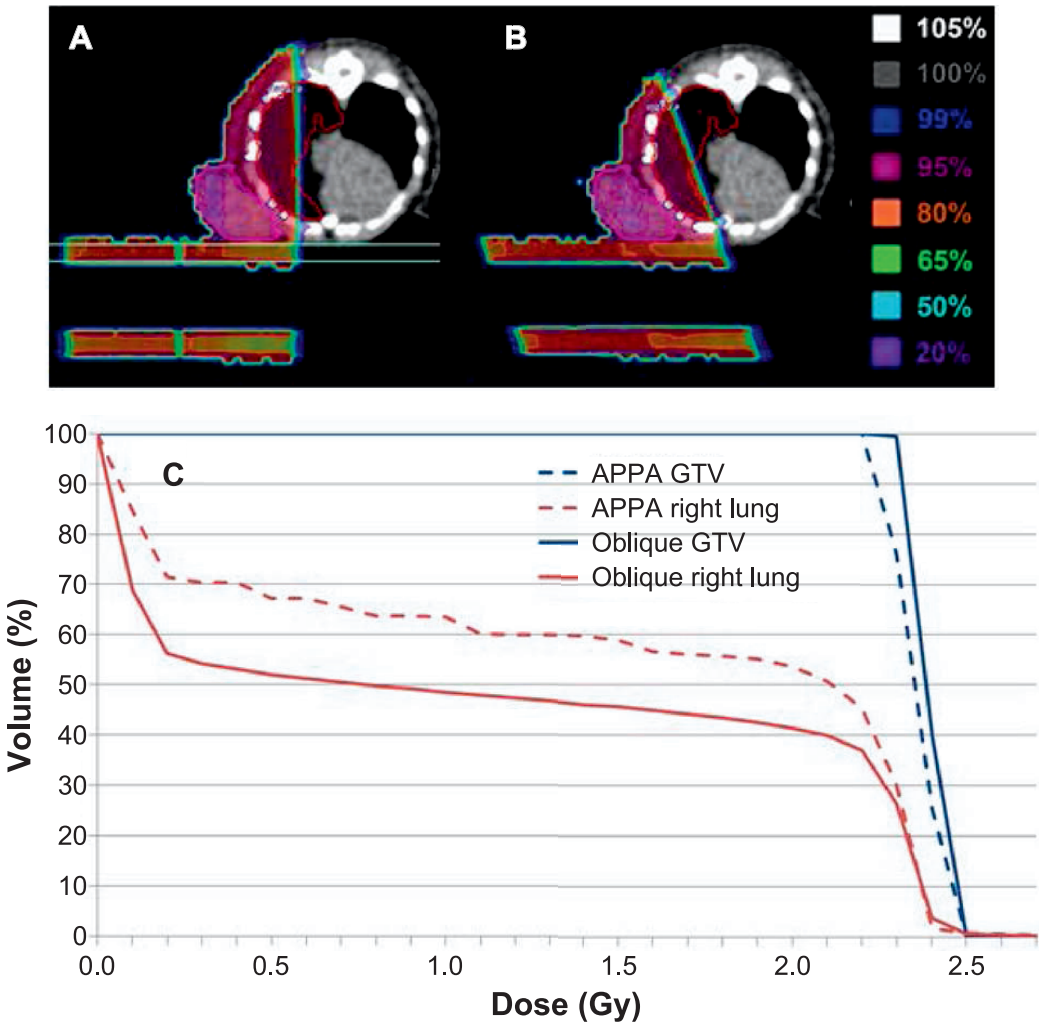

FIG. 5. View of resulting dose distributions in same transverse cut plane for the AP-PA (panel A) and oblique (340°/160°) (panel B) beam arrangements. The CBCT imaging data is taken here from mouse no. 6389 on day 1 and the naïve prescription dose specified from the PDC was 2.52 Gy (15 s per beam). Panel C: DVHs for the GTV and ipsilateral (right-side) lung for the two plans, showing a clear improvement in lung sparing with the oblique arrangement. The field edge is also further away from the spinal column for the oblique plan.

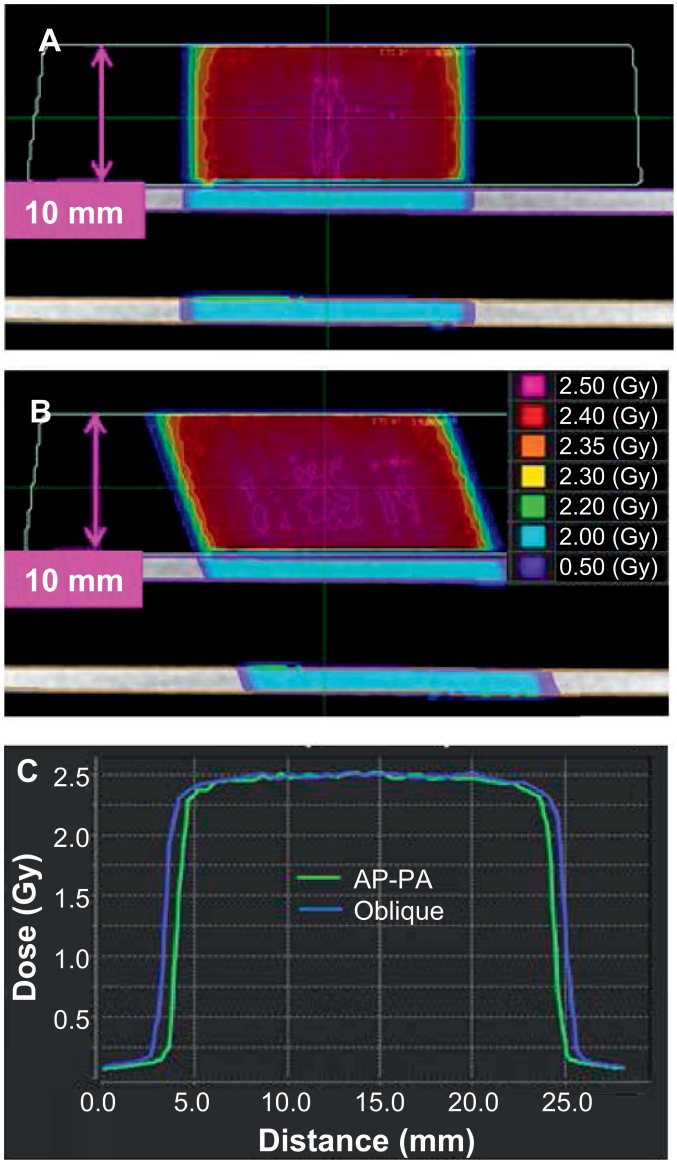

FIG. 6. Transverse cut-plane view of the 3D Monte Carlo dose distribution for 10-mm-thick water phantom with AP-PA (panel A) and oblique 340°/160° (panel B) beam arrangement, calculated on an ''empty'' CBCT scan of the Multiflow bed. The cross-hairs through the phantom coincide with the isocenter location. The water phantom structure (drawn manually and overridden accordingly in the plan) is shown; the two slabs from the Multiflow bed were overridden as polyethylene. The beam timers were set at 15 s (all beams, both plans). Panel C: Corresponding dose-line profiles, sampled laterally along the central axis in the isocentric plane (mid-separation, at depth of 5 mm).

(at the mid-separation depth of 5 mm in the phantom) shows that the two plans resulted in the same dose (approximately 2.5 Gy) being delivered to the center of the phantom, which is in excellent agreement with the PDC prediction (2.52 Gy) in the context of the stochastic fluctuation seen in the dose profiles.

Flank tumor dose-coverage robustness. Figure 7 summarizes the DVH-based analysis of GTV (flank tumor) coverage for all treatment fractions under the two scenarios considered, namely using day 1 stage coordinates for fractions 2–5 (Fig. 7A) compared with using daily CBCT-guidance for target positioning (Fig. 7B). Use of a higher-throughput process not involving daily imaging in this cohort would have resulted in significant compromises in GTV coverage in the form of numerous geographical misses for this 20 mm square collimator. These geographic misses all occurred on days 3 or later, with the majority occurring on days 4 or 5. Specific examples of geographic underdosage are provided in Fig. 7C and D, taken from the (overall) worst-case x and z offsets observed in the study (mouse subject no. 6389, days 4 and 5, respectively). With daily CBCT-based IGRT, we observe a relatively tight band of target DVHs (Fig. 7B). The dose covering the GTV volumes was slightly less than the PDC-predicted 2.52 Gy, owing to multiple factors, including the off-axis target alignment (non-flat lateral dose profiles, as can be appreciated in Fig. 6C), reduced scatter due to missing tissue (surrounding the GTV) and tissue heterogeneities. Importantly, for future application of this irradiation model, we can derive a simple normalization factor based on the ''worst-case''-calculated dose covering at least 95% of the GTV (D95%) per fraction. The worst-case D95% of 2.25 Gy was observed on day 1 for subject no. 1157. If we assert that the worst-case D95% should equal 2.52 Gy, which was our naively-specified point-dose prescription from the PDC, this would require a dose renormalization factor of 1.12 (or 12% increase) for beam-on times to be specified in the Monte Carlo treatment planning system (vs. the PDC).

DISCUSSION

In our flank tumor radiation model developmental study involving a cohort of five murine subjects, imaged over five consecutive sham-irradiation sessions, we found that inter-fraction setup error (total offset magnitude) was 3.6 (±1.5) mm for the relatively simple Multiflow bed setup compare with 3.3 (±1.8) mm for the modified Kopf platform incorporating a bite block and Styrofoam cutout. Considering these findings, and the fact that murine subject roll was not mitigated with our modified Kopf device, the Multiflow bed was determined to be a better choice for high-throughput experiments. However, when considering dosimetric plan robustness, we found it essential to perform CBCT imaging on each mouse for each mock irradiation fraction. Furthermore, we derived a normalization factor (1.12) for our 1D PDC that could be applied to our future flank tumor studies using this setup, which would ensure minimum dose coverage by the specified prescription. These dosimetric findings are specifically applicable to: 1. Our treatment planning infrastructure; 2. Our specific choice of immobilization; 3. Our collimator selection; 4. Our beam geometry; and 5. Potentially, the tumor model (and implantation technique). However, a similar validation strategy could be applied broadly across any treatment planning scenario.

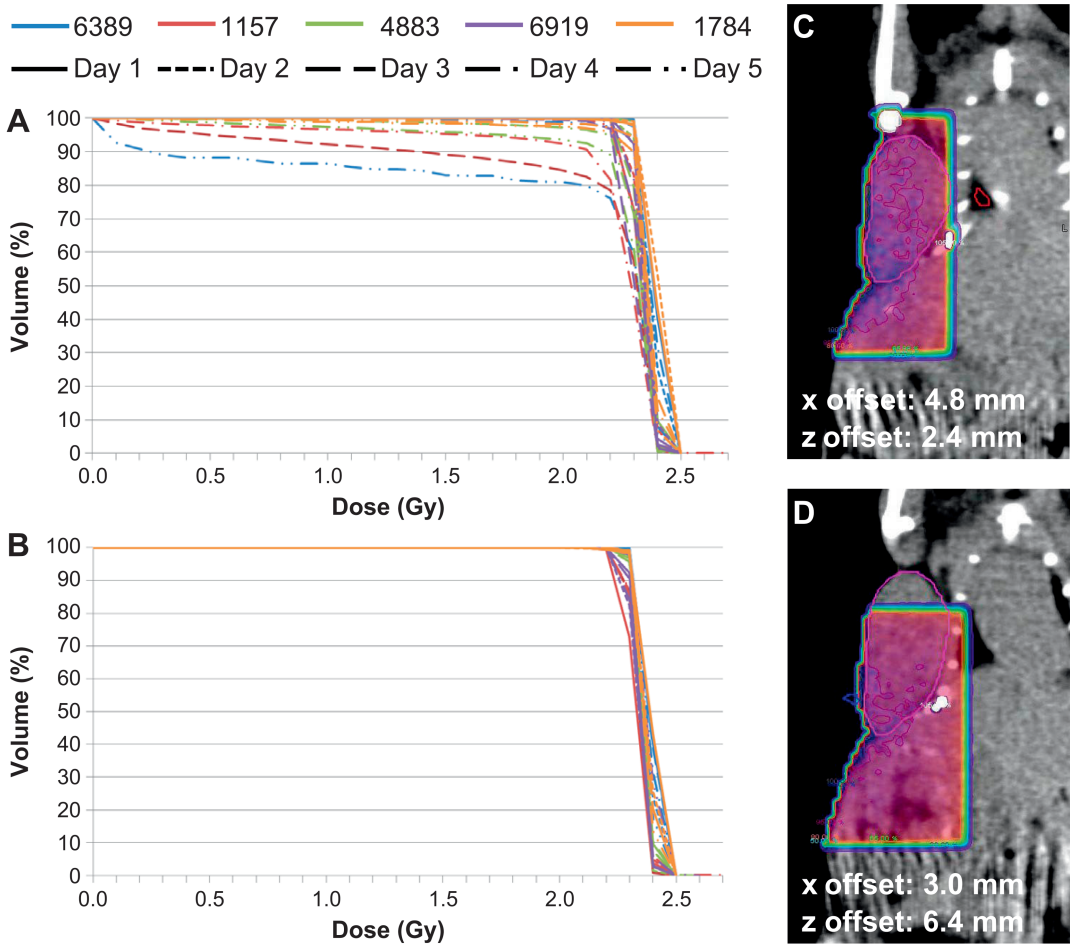

FIG. 7. Panels A and B: Overlaid single-fraction DVHs for the two daily setup scenarios evaluated, namely higher-throughput with use of each subject's day 1 stage coordinates for all fractions (panel A) and daily alignment based on daily CBCT imaging (panel B). There are 25 daily GTV DVHs overlaid on each plot. Each murine subject was assigned a given line color; treatment days 1–5 correspond to solid, short-dashed, long-dashed, dot-dashed and dot-dot-dashed lines, respectively. Panels C and D: Example daily dose distributions (coronal plane) from the high-throughput imaging scenario. Shown are the worst-case x offset [data from subject 6389, day 4 (panel C)] and worst-case z offset [data from subject 6389, day 5 (panel D)]. The GTV contour is visible, with portions at the margin or outside of the high-dose region.

Our system was purchased with most of the fixed collimators available from the vendor. Other collimator sizes. such as 10×10 mm^2 or 15×15 mm^2 or 15 mm diameter (circular) may have been more appropriate for smaller xenografts. For our study, we initially thought that using the larger collimator size of 20×20 mm^2 would allow for sufficiently robust tumor coverage superior-inferiorly. To minimize normal tissue exposure, we chose to use an off-axis isocentric placement.

Beyond this work, examples of setup error evaluation and/or dosimetric plan robustness in the xenograft flank tumor models are difficult to find in the literature. Gan *et al*. used optically stimulated luminescence dosimeters and Gafchromic EBT2 film (also from Ashland Global Holdings, Inc.) to develop a film-only approach to fast dosimetric verification in the context of a high-throughput immobilization device that incorporated cerrobend (Lipowitz's alloy) blocks (to shield normal tissue under a whole-body radiation field) for a kV cabinet irradiator (*8*). However, no multi-subject data were presented in this work. McCarroll *et al*. present a 3D printed immobilizer which was demonstrated to improve rotational setup stability in a cohort of mice. Such a solution could be altered with a cutout to generously accommodate the shape and position of flank tumors, which is an intriguing possibility that we hope to explore in future studies (*9*).

Our study has some limitations related to timing and the simulation of irradiation. The patient-derived tumor line used for the flank tumors was GBM10, which is very aggressive; tumor growth between days 1 and 5 could bias our results. This may be particularly influential when deriving the inter-fraction setup error in the z (superior-inferior) direction, since the landmark was the visually-estimated center of the tumor. Similarly, tumor growth may have biased the comparison between our two immobilization solutions (as the experiments were performed over

successive weeks). Dosimetrically speaking, tumor growth likely exacerbated the effect of observed setup error; the unacceptable spread of DVHs observed in Fig. 7A might have been mitigated somewhat in the actual irradiation context, assuming tumor growth is better constrained. In this context, the results reported here provide a ''worst-case scenario'' of treating a radioresistant tumor that continues to grow during radiation therapy.

Related to the above, our flank tumor volumes were arguably large compared to those in a more typical experiment. Again, because no irradiation occurred and the experiments were conducted over two successive weeks, the tumors had an average maximum tumor volume of 534 mm^3 by day 5 of the second experiment with the Kopf bed. In general, the target volume to begin irradiation of flank tumors in our laboratory is typically between 150 and 200 mm^3. With tumors that are sensitive to radiation, tumor volumes over the duration of treatment will likely not exceed those that we observed. However, arguably, our experiment could be considered as representative for the context of radioresistant cell lines. Clearly, given their geometry, larger tumor volumes pose a challenge in terms of setup reproducibility, which will exacerbate the effect of geometric setup on dosimetric coverage. As we have seen, dosimetric coverage is a key concept that should be investigated in the context of practical, high-throughput flank tumor irradiation to ensure reproducibility of experimental results.

As mentioned as part of the methodology, the X-RAD SmART+ system is capable of 2D fluoroscopic imaging; orthogonally-acquired fluoroscopy imaging could have been evaluated as an alternative to CBCT, assuming it could have provided sufficient visibility/contrast for the flank tumors. We chose not to consider this option because of the more subjective alignment information provided in this context (especially with respect to tumor location on the superior-inferior axis). Past anecdotal experience with fluoroscopy has led us to the conclusion that the gantry motion between orthogonal projection pairs (and additional wait time due to imaging detector dark current calibration and shutter motion with this device) does not result in meaningful efficiency gains compared to CBCT. Although, clearly, fluoroscopy can result in imaging dose reductions compared to CBCT given a presumed reduction in the number of acquired X-ray projections.

Also, ideally, we could have evaluated use of the cabinet laser system as a potentially suitable alternative daily alignment scheme, given the implication for higher throughput. Unfortunately, the laser system mounting scheme from the vendor (made of soft 3D-printed plastic) is subject to instability, compromising our ability to maintain an accurate laser calibration. Work is underway to redesign and produce alternate laser mounting brackets, along with a scribed laser calibration phantom. We anticipate that our modifications should enable more accurate, and more stable, laser-to-imaging isocenter calibration; future experiments to evaluate the effectiveness of laser setup for flank tumors are currently being planned.

In addition to those limitations discussed above, Monte Carlo dose calculations, even when properly commissioned, have limitations in the small-animal irradiator context. These limitations are derived from inaccurate modeling of the X-ray source (focal-spot) geometry and inaccuracies with respect to material definition (*10, 11*). The focal spot issue can be significant for small collimators (of comparable size in relationship to the focal spot) but is less relevant for collimation sizes similar to the 20 mm square used in this study. In the kV X-ray context, because of strong effective Z sensitivity, owing mainly to the photoelectric effect, material definition inaccuracies can lead to significant dose calculation inaccuracy (*1*). Here we employed a set of standard ICRU/ICRP tissues (lung, tissue, bone), but it is unclear how accurate these human-derived material definitions are in the murine context.

CONCLUSION

This work provides an investigational approach that can be readily mimicked for laboratories working on new radiation models in the context of modern micro-IGRT platforms. For purposes of efficiency, simple 1D dose calculators are heavily relied upon in preclinical studies. Here we described an approach to bridge the gap between an efficient 1D method for dose determination and a modern 3D (but clearly lower-throughput) treatment planning capability. In our study, using two hypothetical immobilization solutions for single-mouse flank tumor mock irradiation with a given square collimator, we showed that dosimetric robustness demanded a paradigm of daily CBCT imaging for each specimen. We also looked at setup accuracy differences between these two immobilization scenarios and found that the simpler device, specifically the Multiflow bed incorporating a nose cone for anesthesia, was suitable for our needs in terms of accuracy and also preferable in terms of setup efficiency (since no bite block was required).

ACKNOWLEDGMENT

This work was supported, in part, by the National Institutes of Health (NIH grant no. U01CA 227954).

Received: September 23, 2019; accepted: December 2, 2019; published online: December 26, 2019

REFERENCES

1. Verhaegen F, Granton P, Tryggestad E. Small animal radiotherapy research platforms. Phys Med Biol 2011; 56:R55–83.
2. Walb MC, Carlson BL, Sarkaria JN, Tryggestad EJ. Quantifying the setup uncertainty of a stereotactic murine micro-image guided radiation therapy system. Br J Radiol 2019; 92:20180487.
3. Stewart JM, Ansell S, Lindsay PE, Jaffray DA. Online virtual isocenter based radiation field targeting for high performance small animal microirradiation. Phys Med Biol 2015; 60:9031–46.

4. Clarkson R, Lindsay PE, Ansell S, Wilson G, Jelveh S, Hill RP, et al. Characterization of image quality and image-guidance performance of a preclinical microirradiator. Med Phys 2011; 38:845–56.
5. Ma CM, Coffey CW, DeWerd LA, Liu C, Nath R, Seltzer SM, et al. American Association of Physicists in Medicine. AAPM protocol for 40–300 kV x-ray beam dosimetry in radiotherapy and radiobiology. Med Phys 2001; 28:868–93.
6. van Hoof SJ, Granton PV, Verhaegen F. Development and validation of a treatment planning system for small animal radiotherapy: SmART-Plan. Radiother Oncol 2013; 109:361–6.
7. Rogers DW, Faddegon BA, Ding GX, Ma CM, We J, Mackie TR. BEAM: a Monte Carlo code to simulate radiotherapy treatment units. Med Phys 1995; 22:503–24.
8. Gan GN, Altunbas C, Morton JJ, Eagles J, Backus J, Dzingle W, et al. Radiation dose uncertainty and correction for a mouse orthotopic and xenograft irradiation model. Int J Radiat Biol 2016; 92:50–6.
9. McCarroll RE, Rubinstein AE, Kingsley CV, Yang J, Yang P, Court LE. 3D-printed small-animal immobilizer for use in preclinical radiotherapy. J Am Assoc Lab Anim Sci 2015; 54:545–8.
10. Tryggestad E, Armour M, Iordachita I, Verhaegen F, Wong JW. A comprehensive system for dosimetric commissioning and Monte Carlo validation for the small animal radiation research platform. Phys Med Biol 2009; 54:5341–57.
11. Verhaegen F, Dubois L, Gianolini S, Hill MA, Karger CP, Lauber K, et al. ESTRO ACROP: Technology for precision small animal radiotherapy research: Optimal use and challenges. Radiother Oncol. 2018; 126: 471–8.